PHYSICAL REVIEW B VOLUME 11, NUMBER 12 15 JUNE 1975

Theoretical and experimental studies of the second-order Raman spectra of CsCl, CsBr, and CsI†

B. S. Agrawal, R. D. Kirby, and J. R. Hardy
Behlen Laboratory of Physics, University of Nebraska, Lincoln, Nebraska 68508
(Received 11 March 1974)

Measurements of the second-order Raman spectra of CsCl, CsBr, and CsI have been made at both 300 and 80 °K. From these the three independent spectral components, A_{1g}, E_g, and T_{2g}, have been determined for all three crystals at both temperatures. A theoretical interpretation of these data has been carried out using the phenomenological Born-Bradburn model to describe the Raman polarizability tensor and the deformation-dipole model to provide the lattice-dynamical eigendata. We have found it possible to obtain an excellent description of the observed spectra retaining 16 of the first- and second-neighbor polarizability derivatives in the Born-Bradburn expressions for the elements of the polarizability tensor. We have also found that only three of these need be retained to obtain a good semiquantitative fit to the observed spectra.

I. INTRODUCTION

With the advent of modern laser Raman spectrometers Raman scattering has become a standard technique for studying elementary excitations in solids.

However, while much emphasis has been placed on the study of first-order Raman scattering by phonons, considerably less emphasis has been placed on the study of the second-order spectra. This is unfortunate since, in the case of centrosymmetric structures such as the cesium-chloride lattice, first-order scattering is forbidden and thus studies of the second-order spectra are the only means of probing the lattice dynamics of these materials by inelastic light scattering unless one activates the first-order spectra by the introduction of impurities. It is only recently that experiments of this type have been carried out with the emphasis being laid on obtaining information concerning the dynamics of the host lattice.[1] Other studies[2] of this type have been primarily concerned with obtaining information about the defects themselves.

In this present paper we shall be reporting both experimental and theoretical results on the second-order spectra of CsCl, CsBr, and CsI. This work represents the extension to the theoretical study of the second-order Raman spectra of the cesium halides techniques that have been developed and refined over the past five or six years.[3–7]

The original formalism was developed by Born and Bradburn[8] in 1947 when they introduced the idea of expressing the crystal polarizability as a power series in the nuclear displacements. This is a valid approximation provided the frequency of the exciting radiation is significantly less than that of the lowest electronic transition frequency. The predicted second-order Raman spectra are continuous since they involve the excitation of all possible combinations of two phonons with equal and opposite wave vectors. The intensity of any given combination is weighted by a coefficient which is expressible in terms of the second derivatives of the crystal polarizability with respect to pairs of nuclear displacements. This approach will be described in detail in Sec. III of this paper.

Born and Bradburn were forced to make certain simplifying assumptions, since they did not have today's computational facilities. Thus they assumed that the coefficients had the same values for all combinations as they had for those at the symmetry point at the center of the (111) zone face. More recently Cowley and co-workers[9,10] have used extensions of the shell model to estimate the polarizability derivatives, the most exhaustive and recent studies of this kind being the work of Pasternak *et al.*[11]

In the program mentioned earlier we have followed the alternative route of using the general Born-Bradburn approach, retaining these polarizability derivatives as variable parameters and choosing them to give us the best possible fit to the experimental results. This procedure is described in detail in Sec. IV and in Sec. V we discuss the significance of our results. We also discuss the relation of our present work to older calculations[12–14] which correlated the structure of the observed Raman spectra with that of the two-phonon densities of states and we shall see that the present more sophisticated approach is essential now that the experimental technique provides reliable information about the polarization and intensity of the scattered light.

II. EXPERIMENT

The Raman spectra of CsCl, CsBr, and CsI were measured using a Coherent Radiation model-52 argon-ion laser and a Spex model-1401 double

TABLE I. List of scattering geometries employed, their associated Raman intensities, and the appropriate group-theoretic designations of these intensities.

Crystal	Propagation direction Incident	Propagation direction scattered	Polarization direction Incident	Polarization direction scattered	Raman intensity	Group-theoretic classification
CsCl	[110]	[$\bar{1}$10]	[001]	[001]	I_1	$I(A_{1g})+I(E_g)$
	[110]	[$\bar{1}$10]	[$\bar{1}$10]	[110]	I_4	$\frac{3}{4}I(E_g)$
	[110]	[$\bar{1}$10]	[001]	[110]	I_2	$I(T_{2g})$
CsBr	[001]	[$\bar{1}$10]	[110]	[110]	I_3	$I(A_{1g})+\frac{1}{4}I(E_g)+I(T_{2g})$
	[001]	[$\bar{1}$10]	[$\bar{1}$10]	[110]	I_4	$\frac{3}{4}I(E_g)$
	[001]	[$\bar{1}$10]	[110]	[001]	I_2	$I(T_{2g})$
CsI	[110]	[001]	[$\bar{1}$10]	[$\bar{1}$10]	I_3	$I(A_{1g})+\frac{1}{4}I(E_g)+I(T_{2g})$
	[110]	[001]	[$\bar{1}$10]	[110]	I_4	$\frac{3}{4}I(E_g)$
	[110]	[001]	[001]	[$\bar{1}$10]	I_2	$I(T_{2g})$

monochrometer in conjunction with photon-counting electronics. All spectra to be presented here were obtained using the 90° scattering geometries listed in Table I. Only three geometries were used for each crystal but, as will be seen later, these are sufficient to determine the three independent spectral intensities which are consistent with the cubic symmetry of these crystals (A_{1g}, E_g, and T_{2g}).[15] The relationships between these and the measured intensities are also shown in Table I.

The CsI and CsBr samples were originally obtained from Harshaw Chemical Corp. and were kindly supplied to us by Professor J. W. Weymouth. The CsCl crystal used in this investigation was purchased from the Crystal Growth Facility at the University of Utah. Since the cesium halides do not cleave, all samples were oriented using Laue backscattering techniques. After final polishing the orientations were checked and found to be within ± 3° of the desired orientations.

For CsI and CsCl, the 488-nm line of the argon laser was used for excitation, together with a narrow-band interference filter to eliminate plasma tube fluorescence lines. The CsBr crystal apparently contained unwanted impurities because, when it was illuminated with 488-nm light, it showed a broad and strong fluorescence background. This background increased steadily with time until, after about an hour, it had reached a level of 10^4 counts/sec for a 3-cm^{-1} slit width. This background was not present when the 514.5-nm laser line was used and consequently the CsBr spectra were taken using this as the exciting radiation.

III. THEORY

The general theory of Raman scattering is to be found in Born and Huang[16]; however, in order to specify the problem and for the sake of completeness we shall outline the theory here.

For linearly polarized radiation the Raman scattered intensity per unit solid angle due to transitions from a vibrational state v to another vibrational state v' is given by[16]

$$R(\omega_0+\omega_{vv'})=\frac{\omega_0^4}{2\pi c^3}\sum_{\substack{\alpha\beta\gamma\delta\\ i=1,2}} n_\alpha^i n_\beta^i \langle v'|P^*_{\alpha\gamma}|v\rangle \times\left(1+\frac{\omega_{vv'}}{\omega_0}\right)^4 \langle v|P_{\beta\delta}|v'\rangle {}^-E_\gamma {}^+E_\delta \,. \quad (1)$$

In this formula ω_0 is the angular frequency of the incident light; $\omega_{vv'}=(E_v-E_{v'})/\hbar$, where E_v and $E_{v'}$ are the energies of the vibrational states v and v', respectively; c is the velocity of light; Greek subscripts refer to components along the cube axes; $\vec{n}^1$ and $\vec{n}^2$ are orthogonal unit vectors in a plane perpendicular to the scattering direction; $P_{\alpha\beta}$ is the electronic polarizability tensor; ${}^-E_\gamma$ and ${}^+E_\delta$ are the components of the electric vector of the incident light.

When the levels v and v' form a continuous spectrum, as is the case for second- and higher-order Raman scattering, it is necessary to define R in terms of continuous distribution functions $I_{\alpha\gamma,\beta\delta}(\omega)$ as follows:

$$R(\omega_0+\omega_{vv'})=\frac{\omega_0^4}{2\pi c^3}\sum_{\alpha\beta\gamma\delta} n_\alpha^i n_\beta^i I_{\alpha\gamma,\beta\delta}(\omega) {}^-E_\gamma {}^+E_\delta \,,$$

where R is now the intensity scattered per unit frequency if

$$I_{\alpha\gamma,\beta\delta}(\omega)=\sum_{v'}\left(\langle v'|P^*_{\alpha\gamma}|v\rangle\langle v|P_{\beta\delta}|v'\rangle\right)_{\rm av} \times\left(1+\frac{\omega_{vv'}}{\omega_0}\right)^4 \delta(\omega-(\omega_v-\omega_{v'})) \quad (2)$$

and $\omega=\omega_0-\omega_s$, with ω_s being the angular frequency of the scattered light. The subscript av indicates that we have taken the thermal average over the initial states v.

The elements of the polarizability tensor can be expanded as Taylor series in powers of the ionic displacements $\vec{u}(l,k)$. Thus

$$P_{\alpha\beta} = P_{\alpha\beta}^{(0)} + \sum_{lk\gamma} P_{\alpha\beta\gamma}(l, k)\, u_\gamma(l, k) + \frac{1}{2} \sum_{\substack{ll'kk' \\ \gamma\delta}} P_{\alpha\beta\gamma\delta}(ll', kk')\, u_\gamma(l, k)\, u_\delta(l', k') , \tag{3}$$

where l and l' are cell indices (which run from 0 to $N-1$), while k and k' index the two sublattices. The first term on the right-hand side of Eq. (3) gives Rayleigh scattering and the second term gives first-order Raman scattering. For the cesium-chloride structure this term is zero. However, the third term is finite and gives rise to two-phonon (second-order) Raman scattering.

We now express the ionic displacements in terms of plane-wave phonon normal coordinates and thus obtain

$$P_{\alpha\beta}^{(2)} = \frac{1}{2} \sum_{\vec{q}\vec{q}'jj'} P_{\alpha\beta}(jj' \mid \vec{q}, \vec{q}')\, Q(j \mid \vec{q})\, Q(j' \mid \vec{q}') \tag{4}$$

where $\vec{q}$ and $\vec{q}'$ are the phonon wave vectors, j and j' are the branch indices, and $P_{\alpha\beta}(jj' \mid \vec{q}, \vec{q}')$ is given by

$$P_{\alpha\beta}(jj' \mid \vec{q}, \vec{q}') = \sum_{\substack{ll'kk' \\ \gamma\delta}} P_{\alpha\beta\gamma\delta}(\bar{l}, kk') \frac{\sigma_\gamma(k \mid j\vec{q})\, \sigma_\delta(k' \mid j'\vec{q}')}{N(m_k m_{k'})^{1/2}} \times e^{i[\vec{q}\cdot\vec{a}(l,k) + \vec{q}'\cdot\vec{a}(l',k')]} . \tag{5}$$

In Eq. (5) the σ's are the eigenvectors of the Fourier-transformed dynamical matrix, m_k is the mass of the kth type of ion, $\vec{a}(l, k)$ is the position vector of the ion (l, k) in the undistorted lattice and $\bar{l} = l - l'$. This result can be simplified by using the following two requirements:

(a) The crystal must be invariant under an infinitesimal translation. This implies that

$$P_{\alpha\beta\gamma\delta}(ll, kk) = -\sum_{\substack{l'k' \\ (\pm lk)}} P_{\alpha\beta\gamma\delta}(ll', kk') .$$

(b) Since the change in the wave vector of the light during the scattering process is effectively zero, the net crystal momentum of the final-state phonons must also be zero; thus $\vec{q} = -\vec{q}'$.

By using these two results we obtain the following relation:

$$P_{\alpha\beta}(jj' \mid \vec{q}, -\vec{q}) = \sum_{\substack{\bar{l}kk' \\ \gamma\delta}} P_{\alpha\beta\gamma\delta}(\bar{l}, kk') \left(-\frac{\sigma_\gamma(k \mid j\vec{q})\, \sigma_\delta(k \mid j' - \vec{q})}{m_k} + \frac{\sigma_\gamma(k \mid j\vec{q})\, \sigma_\delta(k' \mid j' - \vec{q})}{(m_k m_{k'})^{1/2}} e^{i\vec{q}\cdot\vec{a}(\bar{l}, kk')} \right) . \tag{6}$$

If we now combine Eqs. (2) and (4) we obtain

$$I_{\alpha\gamma,\beta\delta}(\omega) = \frac{\hbar^2}{16} \sum_{qjj'} P_{\alpha\gamma}(jj' \mid \vec{q}, -\vec{q})\, P_{\beta\delta}(jj' \mid \vec{q}, -\vec{q}) \times \left(\frac{\omega_0 \pm \omega_j(\vec{q}) \pm \omega_{j'}(-\vec{q})}{\omega_0} \right)^4 \delta(\omega \pm \omega_j(\vec{q}) \pm \omega_{j'}(-\vec{q})) \times \frac{1}{\omega_j(\vec{q})\, \omega_{j'}(-\vec{q})} \{ [n(\omega_j(\vec{q})) + \tfrac{1}{2} \pm \tfrac{1}{2}] [n(\omega_{j'}(-\vec{q})) + \tfrac{1}{2} \pm \tfrac{1}{2}] \} , \tag{7}$$

where $n(\omega_j(\vec{q}))$ is the Bose-Einstein occupation number for an oscillator of angular frequency $\omega_j(\vec{q})$. The plus (minus) signs corresponds to phonon creation (destruction). We shall consider only the Stokes spectra which are obtained by taking either $(++)$ or $(+-)$ subject to the condition that $\omega_j(\vec{q}) > \omega_{j'}(-\vec{q})$.

In order to specify the second-order Raman spectra of a cubic crystal completely one only needs to calculate I_{xxxx}, I_{xyxy}, and I_{xxyy}.

The polarizability tensor referred to the cube axes has the form

$$P_{\alpha\beta}(jj' \mid \vec{q}, -\vec{q}) = \begin{pmatrix} P_{xx} & P_{xy} & P_{xz} \\ P_{yx} & P_{yy} & P_{yz} \\ P_{zx} & P_{zy} & P_{zz} \end{pmatrix} ,$$

and the corresponding intensity matrix is given by

$$I_{\alpha\beta\gamma\delta} = \begin{pmatrix} I_1 & I_2 & I_2 \\ I_2 & I_1 & I_2 \\ I_2 & I_2 & I_1 \end{pmatrix} ,$$

where

$$\begin{aligned} I_1 &= I_{xxxx} = I_{yyyy} = I_{zzzz} = \tfrac{1}{3}(P_{xx}^2 + P_{yy}^2 + P_{zz}^2) , \\ I_2 &= I_{xyxy} = I_{xzxz} = I_{yzyz} = \tfrac{1}{3}(P_{xy}^2 + P_{yz}^2 + P_{zx}^2) . \end{aligned} \tag{8}$$

The actual scattering geometries employed in the present work are shown in Table I. Thus we need the two additional intensities I_3 and I_4 defined as follows:

$$\begin{aligned} I_3 &= \tfrac{1}{2}(I_{xxxx} + I_{xxyy} + 2I_{xyxy}) , \\ I_4 &= \tfrac{1}{2}(I_{xxxx} - I_{xxyy}) , \end{aligned} \tag{9}$$

where

$$I_{xxyy} = \tfrac{1}{3}(P_{xx} P_{yy} + P_{yy} P_{zz} + P_{zz} P_{xx}) .$$

These results are obtained by expressing the scattering intensities for the various 90° geometries actually employed in terms of those referred to the $\langle 100 \rangle$ cube axes.

In group-theoretical notation the intensities I_1, I_2, I_3, and I_4 are related to those associated with the three irreducible representations of the symmetric polarizability tensor (A_{1g}, E_g, and T_{2g}) as follows [different authors use different numerical prefactors in their definitions of $I(E_g)$]:

$$\begin{aligned} I_3 &= I(A_{1g}) + \tfrac{1}{4} I(E_g) + I(T_{2g}) , \\ I_2 &= I(T_{2g}) , \\ I_1 &= I(E_g) + I(A_{1g}) , \\ I_4 &= \tfrac{3}{4} I(E_g) . \end{aligned} \tag{10}$$

TABLE II. Symmetry operations.

(a). nn bonds					
Class of symmetry operation	E	$C_3^{\pm}$	σ_1	σ_2	σ_3
Class order (h_K)	1	2	1	1	1
Angle (θ) of rotation	0° or 360°	120° or 240°	0°	0°	0°
Sign	+	+	−	−	−
Character of symmetry operation R, $\psi_K(R)$	54	0	2	2	2
$h_K\psi_K(A_{1g})\,\psi_K(R)$	54	0	2	2	2

(b). nnn (++) or (− −) bonds					
Class of symmetry operation	E	C_2	$2C_4$	$2\sigma_V$	$2\sigma_{V'}$
Class order (h_K)	1	1	2	2	2
Angle (θ) of rotation	0° or 360°	180°	90°	0°	0°
Sign	+	+	+	−	−
Character of symmetry operation R, $\psi_K(R)$	54	2	0	2	2
$h_K\psi_K(A_{1g})\,\psi_K(R)$	54	2	0	4	4

Thus the problem of calculating the Raman intensities reduces to that of calculating $P_{\alpha\alpha}$ and $P_{\alpha\beta}$. This requires a complete knowledge of the polarizability coefficients $P_{\alpha\beta\gamma\delta}(\bar{l}, kk')$. These coefficients form the elements of a fourth rank tensor.

However, since this tensor is symmetric in α and β the number of independent elements is reduced to 54. We will retain only those coefficients which involve nearest-neighbor (nn) and next-nearest-neighbor (nnn) bonds. The number of independent coefficients can be further reduced by the use of point-group symmetry operations. The appropriate operations for nn and nnn bonds are shown in Tables II(a) and II(b), respectively. The number of distinct elements is given by the number of times, $m(A_{1g})$, the one-dimensional totally symmetric irreducible representation occurs in the reducible representation formed from the polarizability coefficients. This is given by[17]

$$m(A_{1g}) = \frac{1}{g} \sum_K h_K \psi_K(A_{1g})\,\psi_K(R)\ , \tag{11}$$

where h_K is the order of the Kth class, g is the order of the group; the character $\psi_K(R)$ can be evaluated using the result that

$$\psi_K(R) = (4\cos^2\theta \pm 2\cos\theta)(4\cos^2\theta \pm 4\cos\theta + 1)\ , \tag{12}$$

where θ is the angle of rotation associated with the symmetry operation (R). The plus or minus signs are used according to whether R is a pure rotation or a rotation-reflection.

From the Tables II(a) and II(b) it can be seen that there must be ten polarizability coefficients for a nn bond, eight for nnn (++) bond, and eight for a nnn (− −) bond. Thus one has, in general, 26 polarizability coefficients for crystals having the cesium-chloride structure. It is interesting to note that, as a result of the different point-group symmetry of the sodium-chloride structure, there are eight coefficients for the nn bonds and 15 each for nnn (++) bonds and nnn (− −) bonds for this structure.

Since we are now left with a total of 26 coefficients we have endeavored to reduce this number by physical arguments. Thus we have set equal to zero those coefficients for which neither γ nor δ corresponds to the axis of the bond. This implies that the polarizability is only significantly affected when there is a direct change in bond length. This reduces the total number of parameters to 16 but leaves the number of nn parameters unchanged.

IV. CALCULATION AND RESULTS

In order to carry out calculations using the formalism we have described we need phonon frequencies and eigenvectors. These were computed using a deformation dipole model for which the short-range forces are restricted to act only between nearest-neighbor unlike ions.[18] We use a sample of 64 000 evenly spaced $\vec{q}$ vectors within the first Brillouin zone. Thus we generate histograms for the various spectra. A histogram step size of 2 cm^{-1} was used; this is comparable with the experimental resolution (3–4 cm^{-1}).

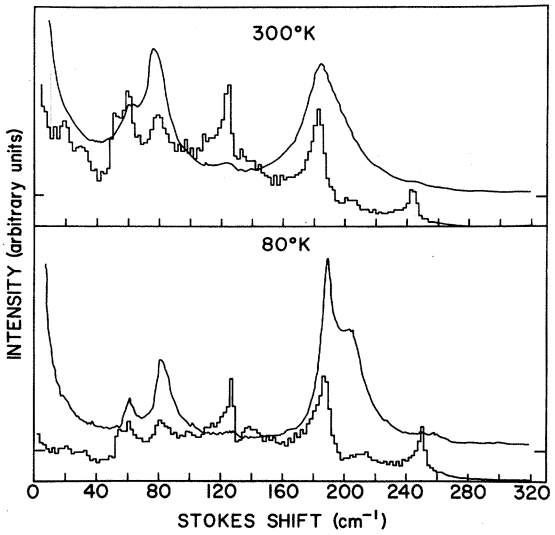

FIG. 1. Computed two-phonon densities of states for CsCl together with the measured I_1 spectra. Since the latter have no T_{2g} component, the theoretical spectra show structure which is absent from the measured I_1 spectra. The smooth curves are the experimental spectra, while the histograms represent the theoretical spectra.

Initially we assume that the polarizabilities $P_{\alpha\beta}(jj'|\vec{q},-\vec{q})$ in Eq. (7) are constant. The two-phonon densities of states thus computed are shown in Figs. 1–3 for CsCl, CsBr, and CsI. On these figures we also show the measured I_1 or I_3 spectra.

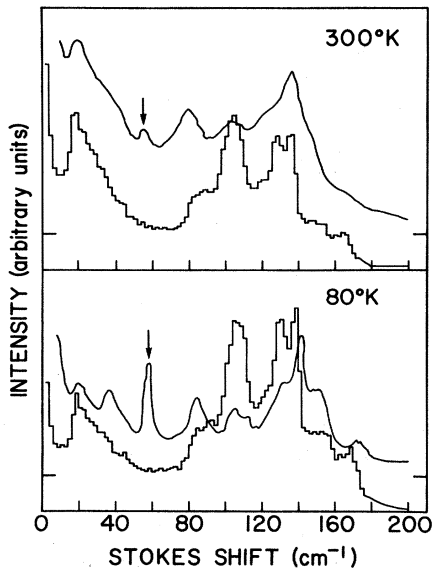

FIG. 2. Computed two-phonon densities of states together with the measured I_3 spectra for CsBr. The smooth curves are the experimental spectra, while the histograms represent the theoretical spectra. The peaks marked by the arrows are due to defect-activated first-order scattering (see text).

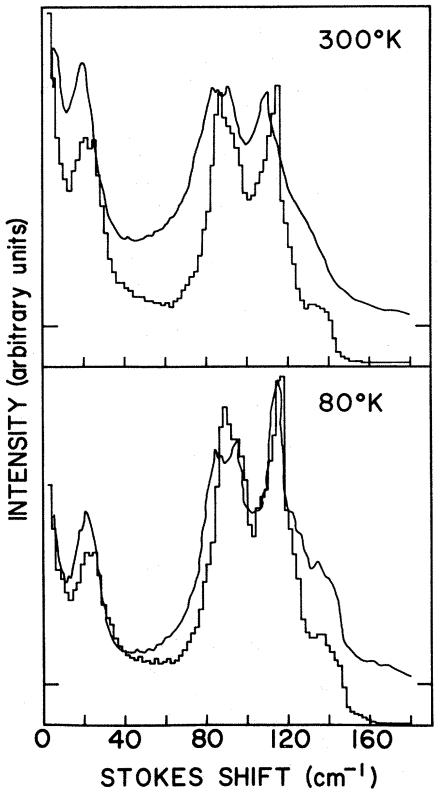

FIG. 3. Computed two-phonon densities of states together with the measured I_3 spectra for CsI. The smooth curves are the experimental spectra, while the histograms represent the theoretical spectra.

It is apparent that this oversimplified approach reproduces the most distinct peaks in the observed spectra in a qualitative fashion but quantitative agreement is poor.

It is thus necessary to refine the theory and express $P_{\alpha\beta}(jj'|\vec{q},-\vec{q})$ in terms of the nn and nnn polarizability coefficients.

In Table III we list the coefficients which have been retained in our calculations and indicate the spectral components to which they contribute. The numerical values are those which give the best agreement between theory and experiment and were determined by a least-squares fit supplemented by specific modifications designed to improve the quality of fit in specific spectral regions.

As can be seen from the figures the fits that we obtain to the observed spectra are excellent. However, the parameters so determined have no clear physical significance and are probably not unique. Thus we need to proceed further in order to obtain a more meaningful understanding of our results. As a first stage, in order to give some physical significance to the numerical values, we have examined the contributions to the various spectra of each individual coefficient. In this way we have found it possible to divide the coefficients into

TABLE III. Values of the polarizability coefficients normalized so that $A=1$. Coefficients A through M_5 are determined by the A_{1g} spectra, the remainder by the T_{2g} spectrum.

Polarizability coefficient $P_{\alpha\beta\gamma\delta}(\bar{l}, kk')$	Bonds	CsCl	CsBr	CsI
$A=P_{xxxx}, P_{yyyy}, P_{zzzz}$	+ −	1.00 ± 0.065	1.00 ± 0.143	1.00 ± 0.045
$D=P_{xxyy}, P_{xxzz}, P_{zzyy}, P_{yyxx}, P_{yyzz}, P_{zzxx}$	+ −	−0.09 ± 0.015	−0.14 ± 0.067	0.02 ± 0.005
$B=P_{xxxy}, P_{xxxz}, P_{zzzy}, P_{yyyx}, P_{yyyz}, P_{zzzx}$	+ −	−0.52	0.07	0.44
$C=P_{xxzz}, P_{zzyz}, P_{yyxy}, P_{yyzy}, P_{xxyx}, P_{zzxz}$	+ −	−0.84	−0.01	−0.07
$E=P_{xxyz}, P_{xxzy}, P_{zzyx}, P_{yyxz}, P_{yyzx}, P_{zzxy}$	+ −	−0.11	0.04	−0.36
$P_1=P_{xxxx}$	+ +	−2.57	1.97	−4.38
$P_5=P_{yyxx}, P_{zzxx}$	+ +	−1.62	0.24	−1.37
$M_1=P_{xxxx}$	− −	−0.69	−1.18	0.34
$M_5=P_{yyxx}, P_{zzxx}$	− −	0.33	−1.94	−1.42
$G=P_{xyxy}, P_{xzxz}, P_{zyzy}, P_{yxyx}, P_{yzyz}, P_{zxzx}$	+ −	0.61 ± 0.140	−0.85 ± 0.035	0.45 ± 0.015
$F=P_{xyxx}, P_{xzxx}, P_{zyzz}, P_{yxyy}, P_{yzyy}, P_{zxzz}$	+ −	0.51	−0.14	−0.12
$H=P_{xyxz}, P_{xzxy}, P_{zyzx}, P_{yxyz}, P_{yzyx}, P_{zxzy}$	+ −	0.58	0.29	0.14
$K=P_{xzyx}, P_{zyxz}, P_{yxzy}, P_{xyzx}, P_{yzxy}, P_{zxyz}$	+ −	−0.45	0.14	0.07
$L=P_{xyzz}, P_{xzyy}, P_{zyxx}, P_{yxzz}, P_{yzxx}, P_{zxyy}$	+ −	−0.55	−0.70	−0.29
$P_8=P_{zxxz}, P_{xyxy}$	+ +	−0.08	−0.31	−0.56
$M_8=P_{zxxz}, P_{xyxy}$	− −	−0.65	−1.66	−1.44

three classes:

(i) coefficients which affect one or more spectra strongly and which are thus well defined.

(ii) coefficients which produce smaller but significant effects, which therefore cannot be set equal to zero although, quite often, they can be varied over a considerable range without producing very significant changes in the computed spectra.

(iii) coefficients which can, to a good approximation, be set equal to zero but which are retained in the last refinements of our calculations since they give small detailed improvements in the agreement between theory and experiment. Since their effects are small, their numerical values are even less well defined than those of parameters in class (ii).

CsCl. In Fig. 4 we show the computed and measured A_{1g}, E_g, and T_{2g} spectra for this crystal at 300 °K while in Fig. 5 we show the corresponding data for 80 °K. The A_{1g} spectra cannot be measured directly but have been calculated from I_1 and I_4 using Eqs. (10).

The parameters A, D, and G are in class (i) and are well defined. The parameters P_1, P_5, M_1, M_5 and F, H, K, and L are in class (ii). The parameters B, C, E and P_8, M_8 are in class (iii).

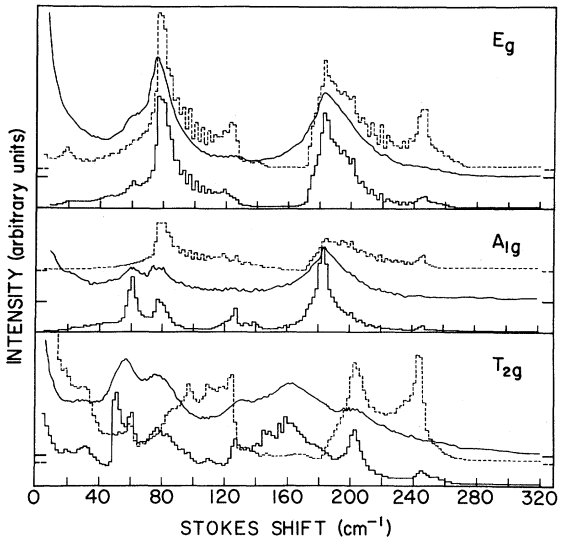

FIG. 4. Experimental and theoretical E_g, A_{1g}, and T_{2g} spectra for CsCl at 300 °K. The A_{1g} and E_g intensities are plotted in the same arbitrary units but the vertical scale on the T_{2g} spectrum has been multiplied by 2 for the sake of clarity. The smooth curves are the experimental spectra, the full histograms are the 16-parameter theoretical spectra, while the broken histograms are the corresponding three-parameter theoretical spectra.

Specifically P_1 and P_5 are required in order to reproduce the observed structure in the A_{1g} and E_g spectra between 60 and 65 cm^{-1}, while M_1 and M_5 are required to fit similar structure between 180 and 190 cm^{-1} in the same two spectra.

B, C, and E could be neglected were it not for their effect on the A_{1g} spectrum between 180 and 190 cm^{-1}, where their inclusion improves the fit over that provided by including only M_1 and M_5.

G is well defined by the T_{2g} spectrum, while F, H, K, and L have to be retained to reproduce some of the more significant subsidiary structure in this spectrum. P_8 and M_8 are retained but their values are very ill defined.

CsBr. Figures 6 and 7 show the computed and measured A_{1g}, E_g, and T_{2g} spectra for this crystal appropriate to 300 °K and 80 °K, respectively. In this case the A_{1g} spectrum has been derived from I_3, I_4, and I_2.

The parameters A, D, and G are well defined and are thus in class (i). The parameters P_1, P_5, M_1, M_5 and P_8, M_8 are in class (ii), while the parameters B, C, E and F, H, K, and L belong to class (iii).

P_1 and P_5 must be retained in order to reproduce the structure observed in E_g and A_{1g} spectra between 100 and 115 cm^{-1}, while M_1 and M_5 are required to fit structure between 170 and 175 cm^{-1}.

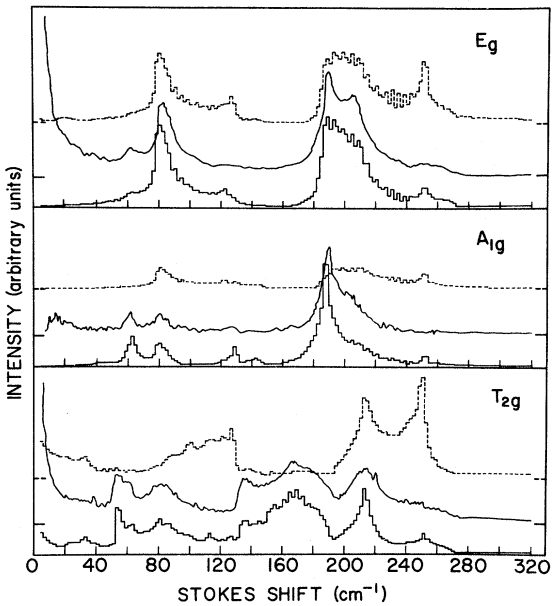

FIG. 5. Experimental and theoretical E_g, A_{1g}, and T_{2g} spectra for CsCl at 80 °K. The A_{1g} and E_g intensities are plotted in the same arbitrary units but the vertical scale on the T_{2g} spectrum has been multiplied by 2 for the sake of clarity. The smooth curves are the experimental spectra, the full histograms are the 16-parameter theoretical spectra, while the broken histograms are the corresponding three-parameter theoretical spectra.

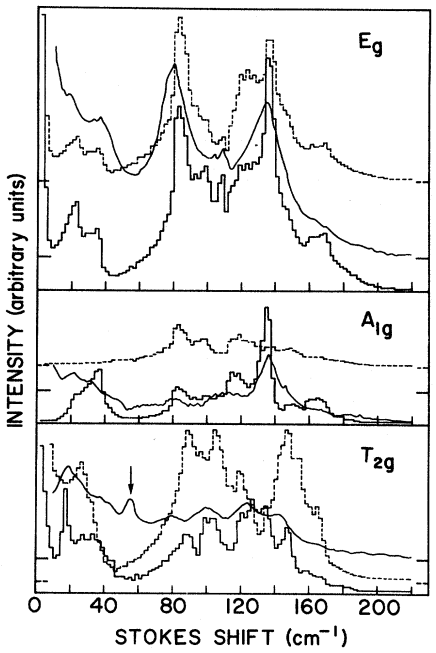

FIG. 6. Experimental and theoretical E_g, A_{1g}, and T_{2g} spectra for CsBr at 300 °K. Intensities are given in the same arbitrary units for all three spectra. The smooth curves are the experimental spectra; the full histograms are the 16-parameter theoretical spectra, while the broken histograms are the corresponding three-parameter theoretical spectra. The peak marked by the arrow is due to defect-activated first-order scattering (see text).

B, C, and E could be neglected; they are retained to refine the ultimate fit but their values are very poorly defined.

G is well defined by the T_{2g} spectrum, while P_8 and M_8 have to be retained in order to reproduce some of the more significant features of the observed spectrum. F, H, K, and L have been retained in the last refinements.

It will be observed that the measured spectra show sharp strong peaks at 55 cm^{-1} (300 °K) and 59 cm^{-1} (80 °K) which are not reproduced by the theory nor are they present in the two-phonon densities of states (Fig. 2). However, earlier calculations of the one-phonon densities of states[19] do show strong peaks at these frequencies. This led us to suspect that these peaks are defect-activated single-phonon scattering. To check this we computed temperature-weighted one-phonon densities of states and we indeed found that the ratio of the peak intensities, so calculated, agreed with the ratio of the experimental intensities. This result confirms our hypothesis and is consistent with the presence of the fluorescence described in Sec. II which is certainly due to some unknown impurity (or impurities) being present in significant quantities.

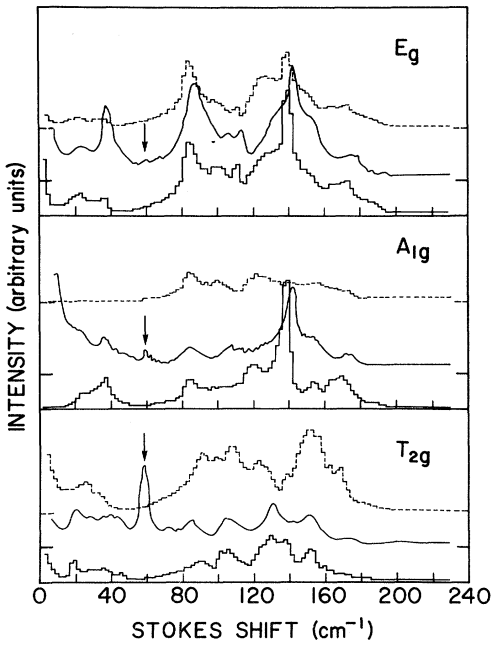

FIG. 7. Experimental and theoretical E_g, A_{1g}, and T_{2g} spectra for CsBr at 80 °K. Intensities are given in the same arbitrary units for all three spectra. The smooth curves are the experimental spectra; the full histograms are the 16-parameter theoretical spectra, while the broken histograms are the corresponding three-parameter theoretical spectra. The peaks marked by the arrows are due to defect-activated first-order scattering (see text).

The disagreement between theory and experiment at low frequencies is almost certainly due to our inability to subtract from the observed signal that component due to a high and unknown background whose origin is Rayleigh scattering and possibly fluorescence.

CsI. Finally, in Figs. 8 and 9 we show the computed and measured 300 °K and 80 °K A_{1g}, E_g, and T_{2g} spectra for this crystal. Again the A_{1g} spectrum has been derived from I_3, I_4, and I_2.

As was the case for CsBr the parameters A, D, and G are in class (i); the parameters P_1, P_5, M_1, M_5 and P_8, M_8 are in the class (ii), while the parameters B, C, E and F, H, K, and L are in class (iii).

We require P_1, P_5, M_1, and M_5 in order to reproduce the main features of the observed E_g and A_{1g} spectra between 90 and 100 cm^{-1}, while M_1 and M_5 perform a similar function for the structure between 115 and 120 cm^{-1}. B, C, and E could be set equal to zero but are retained to refine the agreement between theory and experiment between 90 and 100 cm^{-1}.

G is again well defined by the T_{2g} spectrum, while P_8 and M_8 are retained in order to reproduce some of the more important subsidiary structure in the spectrum. F, H, K, and L are once more used for final refinements.

Once again we have trouble fitting the low-frequency ends of the spectra but this is almost certainly due to the background Rayleigh scattering which we are unable to subtract out. In the case of both the bromide and the iodide this belief is supported by the excellent agreement between theory and experiment over the remainder of the spectra; one would expect a theory that closely reproduces the summation bands to give a reliable prediction of the intensities of the difference bands.

If one makes a comparison between the quality of the agreement which we obtain between theory and experiment for our results with that obtained by Pasternak *et al.*[11] then, as is to be expected, we do much better because we are using 16 parameters where they are using only two. It is thus fair to ask if we can do as well with a comparable number of parameters. Thus we have proceeded in two stages: First we have set equal to zero all

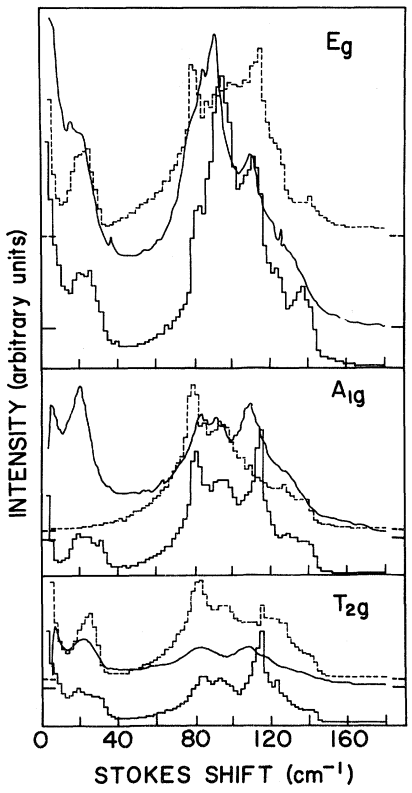

FIG. 8. Experimental and theoretical E_g, A_{1g}, and T_{2g} spectra for CsI at 300 °K. Intensities are given in the same arbitrary units for all three spectra. The smooth curves are the experimental spectra: the full histograms are the 16-parameter theoretical spectra, while the broken histograms are the corresponding three-parameter theoretical spectra.

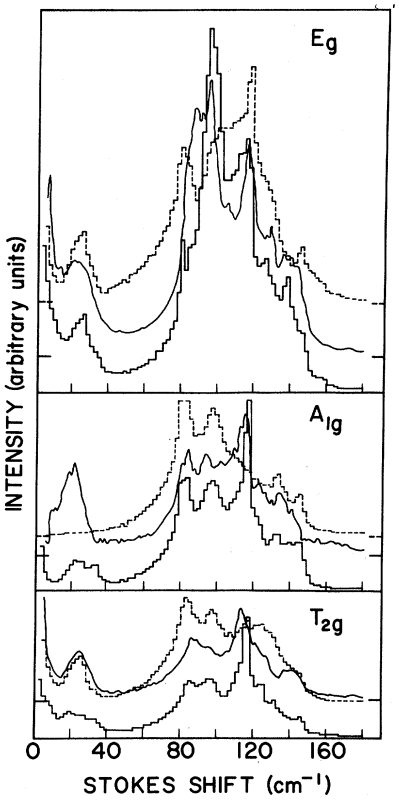

FIG. 9. Experimental and theoretical E_g, A_{1g}, and T_{2g} spectra for CsI at 80 °K. Intensities are given in the same arbitrary units for all three spectra. The smooth curves are the experimental spectra; the full histograms are the 16-parameter theoretical spectra, while the broken histograms are the corresponding three-parameter theoretical spectra.

parameters in class (iii) and finally we have retained only the three parameters A, D, and G which are in class (i).

The result of taking the first step, which leaves nine parameters, is to produce theoretical spectra which are almost indistinguishable from those produced by the 16-parameter model and are thus not shown separately. The one exception to this rule is the T_{2g} spectrum of CsCl, where the agreement is significantly worse and comparable with that provided by the second and final modification.

In Figs. 4–9 we show the spectra predicted by the three-parameter model. For all three crystals we still have good agreement between the experimental and theoretical E_g spectra. For the A_{1g} and T_{2g} spectra the agreement is less good, particularly for the T_{2g} spectrum of CsCl. Even so, the agreement provided by this simple model is in all cases at least as good as that obtained by Pasternak *et al.*[11] This statement remains true if one goes a stage further and sets D equal to zero, since it is always by far the smallest of the three parameters. Since this is the case we conclude that the dominant influence on the Raman spectra is that of the lattice dynamical model because, in the two-parameter limit, the shapes of all the spectra are determined entirely by the predicted eigendata.

In an effort to give a physical interpretation of the relative magnitudes of the polarizability derivatives we proceeded one stage further and made the assumption that the ionic polarizabilities were affected only by changes in the bond lengths. When this assumption was used for the nearest-neighbor bonds it transpired that the nearest-neighbor contributions to the E_g spectra were *identically* zero. This is a consequence of the symmetry of the CsCl structure. Moreover, it was impossible to reproduce the observed E_g spectra using second-neighbor polarizability derivatives alone. The predicted peaks occur in the wrong positions and examination of the algebraic expression for the E_g intensity reveals that this is due to the manner in which zone-boundary combinations are suppressed in the second-neighbor contribution to the E_g spectrum.

Since the analysis of Pasternak *et al.*[11] uses an assumption closely analogous to that we have just discussed, it would appear that an analysis of the cesium-halide spectra using their approach is unlikely to succeed. It is true that their arguments lead them to the conclusion that the parameter $A(P_{xxxx})$ dominates the first-neighbor contribution to the scattering for NaCl structures, but this is only true because the first-neighbor bonds lie along $\langle 100 \rangle$ directions; this is no longer true for the CsCl structure, and consequently the rationale outlined above breaks down. Thus it would appear that the dominance of A indicates that the dependence of the crystal polarizabilities on ionic displacements is very anisotropic, suggesting that the dominant effect is coupling of the displacements to an electronic distortion having ellipsoidal symmetry.

V. CONCLUSION

By employing the Born-Bradburn model we have been able to obtain excellent fits to the measured second-order Raman spectra of all three CsCl structure cesium halides. We have retained the 16 polarizability coefficients allowed by our bond-extension approximation and we have studied their relative significance as described in Sec. IV. In this final section some general remarks about them are in order.

The fact that these parameters are more than adequate to fit the observed spectra implies that the Born-Bradburn model provides a meaningful interpretation of the observed spectra. Moreover we have shown that it is possible to obtain fair to good agreement between theory and experiment using very simple two- or three-parameter models.

This last result points the way to further work, which should be aimed at the study of the relative magnitudes of the parameters by quantum-mechanical calculations.

The fact that our calculations involve both eigenfrequencies and eigenvectors is some indication that our lattice dynamical model predicts both with reasonable accuracy. This is important in view of recent work[20] which shows that one can construct force-constant models which give identical eigenfrequencies by very different eigenvectors.

It will be observed by inspection of Table III that sometimes the second-neighbor parameters are considerably larger than the nearest-neighbor parameters for the same crystal. In spite of this the former are generally classified as being subject to marked uncertainty. This appears to be a consequence of the structure of CsCl. It transpires that in the process of Fourier transformation these coefficients are multiplied by numbers which are at least an order of magnitude smaller than those which multiply the first-neighbor coefficients. Consequently, in order to reproduce significant spectral peaks which are not predicted by the first-neighbor coefficients alone, one has to use large second-neighbor coefficients and their values are ill defined by our minimization program.

An additional reason for individual parameters being ill defined is that the computed spectra are only sensitive to combinations of two or more of them. For example, a particular A_{1g} spectrum defines the sum $B+C+E$ with fair precision, while the E_g spectrum depends on B, C, and E separately. Unfortunately this dependence is not very strong and consequently the individual coefficients are ill defined.

ACKNOWLEDGMENTS

We should like to express our thanks to Professor S. S. Jaswal and Dr. T. P. Sharma for helpful discussions during the course of this work.

---

†Work supported in part by National Science Foundation under Department Development Grant No. GU3163.

[1]R. T. Harley, J. B. Page, Jr., and C. T. Walker, Phys. Rev. B 3, 1365 (1971); Phys. Rev. Lett. 23, 922 (1969); T. P. Martin, J. Phys. C 5, 493 (1972).

[2]R. D. Kirby, Phys. Rev. B 4, 3557 (1972); B. N. Ganguly, R. D. Kirby, M. V. Klein, and G. P. Montgomery, Jr., Phys. Rev. Lett. 28, 307 (1972).

[3]J. R. Hardy, A. M. Karo, I. W. Morrison, C. T. Sennett, and J. P. Russell, Phys. Rev. 179, 837 (1969).

[4]J. R. Hardy and A. M. Karo, Phys. Rev. 168, 1054 (1968).

[5]J. R. Hardy and A. M. Karo, in *Proceedings of the International Conference on Light Scattering Spectra of Solids*, edited by G. B. Wright (Springer-Verlag, New York, 1969), p. 99.

[6]S. S. Jaswal, G. Wolfram, and T. P. Sharma, J. Phys. Chem. Solids 35, 571 (1974).

[7]T. P. Sharma, R. D. Kirby, and S. S. Jaswal, Phys. Rev. B 9, 1971 (1974).

[8]M. Born and M. Bradburn, Proc. R. Soc. A 188, 161 (1948).

[9]R. A. Cowley, Proc. R. Soc. Lond. 84, 281 (1964).

[10]A. D. Bruce and R. A. Cowley, J. Phys. C 5, 595 (1972).

[11]A. Pasternak, E. Cohen, and G. Gilat, Phys. Rev. B 9, 4584 (1974).

[12]A. M. Karo, J. R. Hardy, and I. W. Morrison, J. Phys. (Paris) 26, 668 (1965); S. Ganesan, E. Burstein, A. M. Karo, and J. R. Hardy, J. Phys. (Paris) 26, 639 (1965).

[13]A. M. Karo and J. R. Hardy, Phys. Rev. 160, 702 (1967).

[14]E. Burstein, F. A. Johnson, and R. Loudon, Phys. Rev. 139, A1240 (1965).

[15]Unpublished data taken by W. Bauhofer, M. Buchanan, R. Haberkorn, and T. P. Martin for CsCl, CsBr, and CsI at room temperature are in close agreement with our results. We should like to thank these authors for communicating their results to us.

[16]M. Born and K. Huang, *Dynamical Theory of Crystal Lattices* (Clarendon, Oxford, England, 1954), p. 199.

[17]M. Tinkham, *Group Theory and Quantum Mechanics* (McGraw-Hill, New York, 1964), pp. 18–49.

[18]S. Bhagavantam and T. Venkatarayudu, *Theory of Groups and Its Applications to Physical Problems* (Academic, New York, 1969), pp. 159–170.

[19]B. S. Agrawal and J. R. Hardy, Solid State Commun. 14, 239 (1974).

[20]R. S. Leigh, B. Szigeti, and V. K. Tewary, Proc. R. Soc. A 320, 505 (1970).